Available online at www.sciencedirect.com

jmr&t Journal of Materials Research and Technology

journal homepage: www.elsevier.com/locate/jmrt

Original Article

Facile synthesis of ZnO–Ag nanocomposite supported by graphene oxide with stabilised band-gap and wider visible-light region for photocatalyst application

Saharman Gea [a,b,*], *Suhut A. Situmorang* [a,b], *Nurhaida Pasaribu* [b], *Averroes F.R. Piliang* [a,c], *Boy Attaurrazaq* [a], *Reka Mustika Sari* [a,b], *Khatarina Meldawati Pasaribu* [a,b], *Stergios Goutianos* [d]

[a] *Cellulosic and Functional Materials – Research Centre, Universitas Sumatera Utara, Medan, 20155, Indonesia*
[b] *Department of Chemistry, Faculty of Mathematics and Natural Sciences, Universitas Sumatera Utara, Medan, 20155, Indonesia*
[c] *Department of Physics, Faculty of Mathematics and Natural Sciences, Universitas Sumatera Utara, Medan, 20155, Indonesia*
[d] *Department of Manufacturing and Civil Engineering, Norwegian University of Science and Technology, NO-2802, Gjøvik, Norway*

ARTICLE INFO

Article history:
Received 9 March 2022
Accepted 30 May 2022
Available online 9 June 2022

Keywords:
Electrospinning
Photocatalyst
Graphene oxide
Silver nanoparticles
ZnO

ABSTRACT

The synthesis of zinc oxide (ZnO), with the support of silver (Ag) and Graphene Oxide (GO), was carried out in several stages as a potential photocatalytic material. First, the GO was synthesized from commercial graphite using the Hummers' method, and ZnO and Ag precursors were prepared. The second stage was the electrospinning process, followed by calcination. The solution in the electrospinning process, to produce the nanofibers, was a mixture of polymer (polyvinyl alcohol), zinc acetate, $AgNO_3$, and GO. The fibres produced were thermally treated at 500 C for 2 h. XRD and FTIR analyses confirmed that GO was successfully synthesized from commercial graphite. ZnO and Ag had wurtzite and cubic hexagonal structures based on XRD and TEM characterization. The nanocomposites developed had increased photocatalyst characteristics: low band gap energy, such as 2.98 (ZnO), 2.76 (ZnO–Ag), 2.93 (ZnO-GO), and 2.75 (ZnO–Ag-GO). Furthermore, the nanocomposites had absorption characteristics in the visible light region. Using UV–Visible spectrophotometer, Diffuse Reflectance Spectroscopy, and Photoluminescence, it was explained that the Surface Plasmon Resonance effect possessed by Ag and GO nanoparticles had semiconductor properties that acted as electron trapping, thereby reducing or preventing the occurrence of electron–hole recombination. In conclusion, the ZnO nanocomposites with the addition of Ag and GO could improve the photocatalytic characteristics of ZnO with the potential for direct application in photodegradation of organic and textile waste in water.

* Corresponding author.
E-mail address: s.gea@usu.ac.id (S. Gea).
https://doi.org/10.1016/j.jmrt.2022.05.184

1. Introduction

Water pollution has severe adverse effect on water quality, and a strong negative impact on the aquatic ecosystem [1]. Organic dyes, used in textile, printing, food, and pharmaceutical industries [2] are among the substances that pollute water and therefore affect human life, plants and organisms living in water [3]. These dyes can remain in the environment due to their low biodegradability, and their by-products, present on water, are more toxic even though they are naturally degraded [4]. To overcome this issue, one of the available methods, especially for wastewater containing various contaminants like organic solvents, pharmaceutical waste, pesticides, and other hazardous chemicals [4], is photodegradation based on photocatalysts and ultraviolet (UV) or visible lights. During the photodegradation, advanced oxidation processes (AOPs) occur that are commonly found in semiconductors, so heterogeneous photocatalysts-based semiconductors are widely used in UV/Visible light or artificial lighting [5]. However, the use of metals oxides in semiconductors, in heterogeneous photocatalysts, is not attractive due to high costs and low availability.

Several semiconductor materials are suitable photocatalysts for water treatment such as TiO_2, ZnO, Fe_2O_3, ZrO_2, V_2O_5, Nb_2O_5, and WO_3 [6] due to AOPs characteristics. Among these, ZnO, an n-type semiconductor with a gap energy of ~3.37 eV, has been widely used in water decontamination photocatalysis because of its attractive photocatalytic properties e.g., strong oxidizing ability, chemically and physically stable structure, biocompatibility, non-toxicity, high photosensitivity, low affordability, and high availability [7]. However, the large energy gap in ZnO has led to nonoptimal photocatalytic activity (pollutant oxidation and reduction) due to electron–hole recombination e.g., reduced active species on photocatalyst surface [7]. Therefore, it is important to prevent, through modifications, electron–hole recombination in order to increase ZnO photocatalytic activity.

Chemical deposition of precious metals and support materials on the ZnO surface could overcome the limitations of ZnO characteristics, as well as provide unique properties such as high chemical stability and bio-affinity. Several studies have been conducted to increase ZnO photocatalytic activity, including the addition of dopant [8], metal deposition on the surface of ZnO photocatalyst [9], the use of materials with heterojunctions between ZnO and TiO_2 [10], as well as ZnO and Bi_2WO_6 [11]. The deposition of silver on the ZnO surface could increase the visible light absorption, thereby increasing the photocatalytic activity in Methylene Blue (MB) photodegradation under visible light irradiation [12]. On the other hand, the use of support materials, such as a) carbon-containing materials like activated carbon, graphene oxide, graphene, carbon nanotubes (CNT), and b) carbon quantum dots (CQD), graphene oxide (GO) [3] as dispersants and adsorbents, could increase the surface areas in photocatalysts [4]. Ramos et., al have synthesized a photocatalyst material based ZnO by adding reduced graphene oxide (rGO) as a support material with an improved photodegradation activity of methyl orange [13]. Thus, modification of photocatalyst materials with the addition of sensitizer such as silver and support material can increase the photocatalytic activity.

There is a direct correlation between the structure, shape, and surface area of nanomaterials and their physical/chemical properties, and therefore it is crucial to control these parameters. A study on nanometre-sized photocatalysts, focused on the morphology and sizes of photocatalyst materials, has resulted in decreasing the band gap from 3.24 eV to 3.16 eV [14]. The synthesis of ZnO photocatalyst materials could produce different structures like nanoparticles, nanorods, nanosheets, nanotubes, and nanofibers [15]. In recent years, one-dimensional (1D) ZnO nanofibers have become attractive because of their unique morphological and optoelectronic properties due to large surface areas, making this shape preferred for synthesizing photocatalytic materials [16]. Among the nanofabrication techniques, electrospinning has become one of the most promising techniques for large-scale nanofibers production, where the fibre diameter can be adjusted. Moreover, the produced fibres have large specific surface area and high porosity which both lead to improved photoreduction activities [17]. Pascariu et al., also have synthesized ZnO–SnO_2 nanofibers, by electrospinning, in which the diameter of these fibres was affected by the calcination process, subsequently; the emission properties under UV/Visible-light radiation, changed [18].

In this study, the synthesis of ZnO-GO nanocomposites is proposed via electrospinning method with the deposition of silver nanoparticles, followed by calcination process. The addition of GO is expected to increase the photocatalyst surface area and inhibit the electron–hole recombination process. The addition of GO could also facilitate reactions in water and polar solvents due to the large number of hydrophilic groups in the form of hydroxyl and epoxy [19]. Modifying ZnO, by depositing silver species, is expected to accumulate the active groups of electrons and holes on the surface and react with the adsorbed organic pollutant compounds. In the present work, the effect of silver nanoparticles and the GO addition to the photocatalyst material is studied. The manufacturing of nanofibers via electrospinning method is expected to produce the supporting structure for the calcination process. The calcined nanocomposites are characterized to determine their potential as photocatalytic material.

2. Experimental

2.1. Materials

Zinc acetate dihydrate ($Zn\ OAc)_2.2H_2O$), silver nitrate ($AgNO_3$), polyvinyl alcohol (PVA), $H_2SO_{4(p)}$, $KMnO_4$, H_2O_2, HCl, and deionized water (DI) were purchased from Sigma–Aldrich. Graphite was supplied by a local supplier in Medan, Indonesia. All the materials were analytical grade and used without further purification.

2.2. Synthesis of graphene oxide

The synthesis of graphene oxide (GO) was carried out by using a slightly modified Hummers' method [20]. In brief, first 25 mL of $H_2SO_{4(p)}$ were added into a flask that contained 1 g of graphite, and the mixture was stirred at 10°C for 30 min. Then, 3 g of $KMnO_{4(s)}$ were slowly added to the mixture. The mixture

was stirred for 2 h at 35°C. Next, 50 mL of DI were slowly added, and the mixture was stirred at 80°C for 30 min. Afterwards, 175 ml of DI were added to stop the reaction, and 10 mL of 30% H_2O_2 were finally added to reduce the permanganate residue. The precipitate was collected, and then centrifuged, and washed six times using HCl 1M and water, followed by ultrasonication for 4 h. The produced solid was then dried and stored for further use.

2.3. Synthesis of ZnO, ZnO–Ag, ZnO-GO, and ZnO–Ag-GO

The synthesis route of the nanocomposites consisted of three steps: a) Polymer-based precursor solution preparation for the electrospinning process, b) electrospinning process, and c) calcination process, and the following Fig. 1 illustrates the synthesis steps.

First, PVA was used as the polymer-based precursor solution in the electrospinning process. A 14% of PVA solution was prepared by dissolving 14 g of PVA powder in 100 mL deionized water (DI). Then, this solution was sonicated using an ultrasonic bath (Elmasonic E–15H) for 2 h at 90°C. The sonication was repeated for 24 h at 90°C. A viscous polymeric solution of PVA was obtained for further use, and in this solution, various compositions of $Zn(OAc)_2$ were added. The preparation of the precursor solution was carried out by mixing 10 mL of PVA with 1 g of $Zn(OAc)_2.2H_2O$, and it was stirred to obtain ZnO in a homogeneous state. Meanwhile, ZnO–Ag solution was prepared by adding 3 mL of $AgNO_{3(aq)}$ to PVA-$Zn(OAc)_2$ mixture, and this mixture was stirred until it became homogeneous. As for the ZnO-GO, it was prepared by adding 3 mL of GO solution (2 mg/mL) to PVA-$Zn(OAc)_2$. Finally, the ZnO–Ag-GO was prepared by adding 3 mL of each $AgNO_{3(s)}$ and GO solution (2 mg/mL) to PVA-$Zn(OAC)_2$ mixture.

Secondly, the electrospinning was performed for each precursor solution. The electrospinning setup was consisted of a 10 mL capacity syringe pump, a needle ground collector, and a voltage supply (Fig. S1). Each of the homogenous mixtures, ZnO, ZnO–Ag, ZnO-GO, and ZnO–Ag-GO solution, was loaded into the syringe with 17.5 kV voltage applied at the tip of the needle to form the Taylor cone that would deposit the nanocomposite on the aluminium foil substrate. The distance between the needle and the collector was 10 cm and the feed rate was 1 mL/h. The spun nanofibers were peeled off from the aluminium foil, and stored under vacuum for further use.

Finally, all the nanofibers were calcinated in a furnace in order to obtain nanocomposites as photocatalyst materials. The calcination was performed at 500° for 2 h in open air conditions, and the temperature was selected via the TGA measurement.

2.4. Characterisations

The morphology of nanofibers was analysed by scanning electron microscopy, SEM (JEOL 6060 equipped with EDS instrument), and transmission electron microscopy, TEM. The infrared spectra of the precursors after electrospinning and

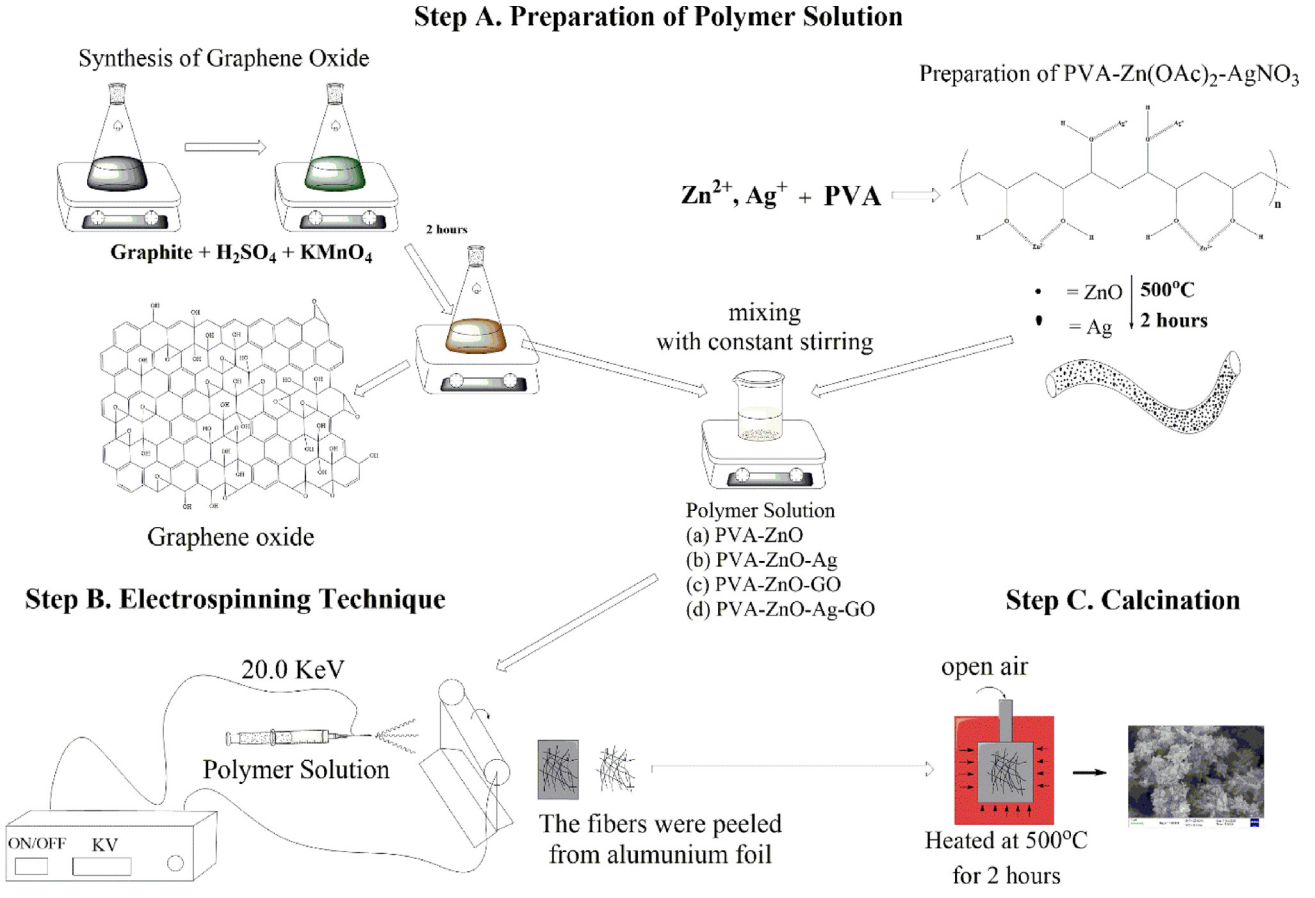

Fig. 1 – Schematic diagram of synthesis routes.

calcination were studied by FTIR (Shimadzu 8201-FC, Kyoto, Japan). The spectra measurements were carried out in the 500-4000 cm^{-1} range. XRD measurements were performed to determine the crystal structure of all nanocomposites (after calcination), and carried out at 40 kV and 40 mA with 1.54 Cu-Kα radiation. The XRD spectra were taken at 2θ in the range of 5–80° with a scanning rate of 0.003°s^{-1}. TGA analysis was performed to examine the thermal properties of the electrospun fibres and it was used to determine the temperature for the calcination process. One of the electrospun fibres was analysed by using DTA/TG Extar II 7300 (Hitachi Medical System, Tokyo, Japan), and then TGA, performed at 30–600°C within inert conditions, was used to determine the decomposition temperature to obtain fine ZnO-GO-Ag. Due to the use of silver, which has similar refractive index to gold, UV–Vis with Diffuse Reflectance Spectron (DRS) was carried out to determine the absorption properties, whereas photoluminescence measurements were performed to investigate the emission characteristics. Finally, the specific surface area of the nanocomposites was measured by Brunaeur-Emmett-Teller (BET) N_2 adsorption–desorption at 77.350 K (Quantachrome QuadraWin ©2000-160).

3. Results and discussion

The oxidation reaction of graphite took place under acidic conditions with the addition of sulfuric acid and potassium permanganate which resulted in a colour change of the mixture from dark green to dark brown (Fig. S2). This was assumed as the oxidation step of graphite sheet which resulted in the formation of functional groups such as alcohols, ketones, carboxylates, and carbonyls. Subsequently, the sheet formed into a graphene oxide sheet with various functional groups. The determination of these groups is shown in Fig. 2.

The FT-IR spectra of GO showed absorption peaks at wavenumbers 3220 cm^{-1} (O–H stretching vibration), 2929 cm^{-1} (C–H stretching vibration), 1883 cm^{-1} (C–H bending vibration), 1699 cm^{-1} (C=O stretching vibration), 1580 cm^{-1} (C=C stretching vibration), 1170 cm^{-1} (C–O stretching vibration), and 1028 cm^{-1} (C–O–C stretching vibration) [19]. The determination of successful synthesis of GO sheets was confirmed via XRD analysis, in which the phase, structure, and crystalline size were measured. Fig. 3 shows the results of XRD analysis of GO samples.

The graphene oxide diffraction pattern indicated the presence of GO as it is shown in Fig. 2, with a strong and wide diffraction peak around 10.4°, a reflection plane (002) and a d-spacing of 8.49 Å. The widened peak and reduced crystallinity compared to graphite could indicate that the GO surface has been intercalated by several oxygen functional groups during the oxidation process [21,22]. Then, the GO sheet is expected to be electron acceptor as additive material.

In performing electrospinning, two preparation steps contributed equally important: (a) the polymer-solution to bind both the Ag and GO, and (b) to initiate the metal ion reduction reactions. The selection of PVA was based on its characteristics that contained polyol groups to bind Zn^{2+} and Ag^{+} ions. Moreover, the polyol also acted as complexing and capping agent that prevented aggregation during the nanoparticle growth process even though the nanoparticles had weak stabilizing properties which could be easily removed by high temperature heating [23]. Our previous study has concluded the presence of silver nanoparticle through Diels–Alder reaction, which showed a reduction of OH and C–O- within the PVA [24]. The second step is the operating set-up of electrospinning, including the feed rate, the distance between collector and syringe pump, and the electrical voltage. As the study employed the 17.5 kV, the nanofibers were expected to be formed, by which the addition of Ag and GO may increase the fibre diameter. Fig. 3 displays a SEM micrograph of electrospun nanofibers of samples ZnO and ZnO–Ag-GO.

Based on Fig. 4, it is confirmed that one-dimensional nanofibers were produced. The nanofibers are connected to each other, forming a porous structure. The average PVA/ZnO and PVA/ZnO–Ag-GO fibre diameter was 62.5 nm and 89.5 nm respectively, which indicated an increase of the diameter due to the presence of Ag and GO. The micrograph of ZnO–Ag-GO (Fig. 4b) displayed much more bead-shapes

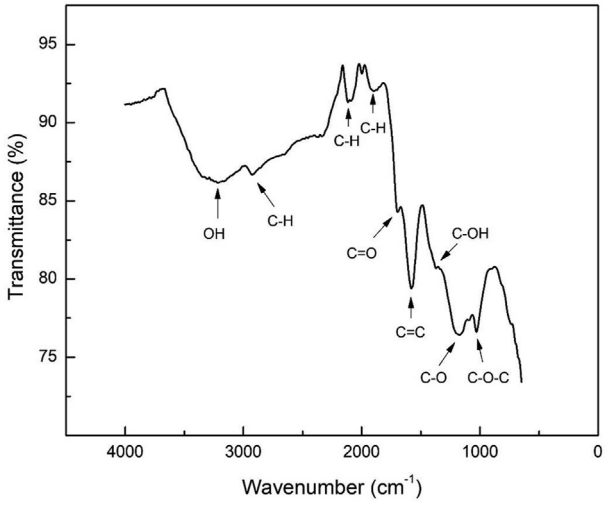

Fig. 2 – FTIR spectra of synthesized graphene oxide (GO).

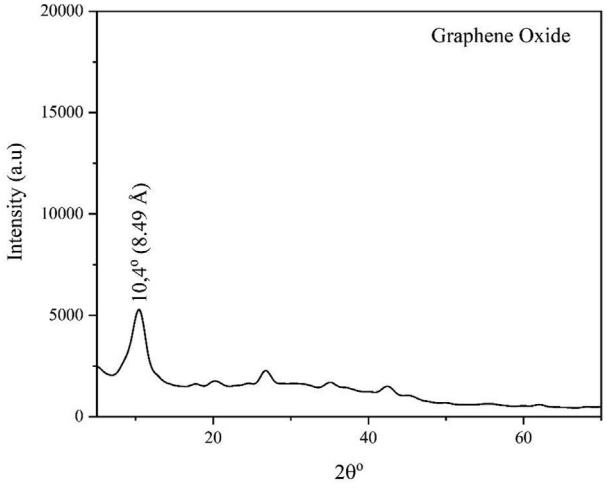

Fig. 3 – X-Ray diffractogram of graphene oxide (GO).

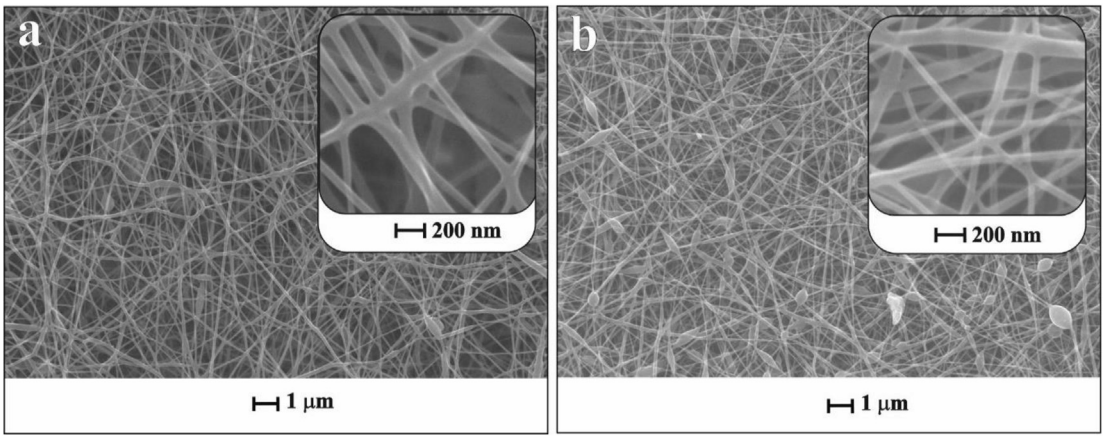

Fig. 4 – SEM micrograph of (a) ZnO, and (b) ZnO–Ag-GO electrospun nanofibers.

on the fibres compared to the PVA/ZnO (Fig. 4a); similar increase in diameter was observed in our previous result for PVA/$AgNO_3$ [24]. These micrographs also confirm that the PVA solution acted as the supporting material to bind the fibres. To investigate materials with photocatalytic properties, the ZnO–Ag-GO nanofibers was selected for TGA measurements due to the presence of Ag and GO as supporting materials. The decomposition temperature that is determined would be used for calcination temperature and the results are given in Fig. 5.

According to Fig. 5, the PVA/ZnO–Ag-GO nanofiber experienced 3 degradation stages. The initial mass reduction by 14% occurred at 100–150°C due to the evaporation of volatile compounds such as water and hydrates from the Zn precursor [14]. The second mass reduction occurred at 300°C by 36%, in which most organic compounds from PVA such as the acetate and nitrate groups in Zn^{2+} and Ag^{+} precursors decomposed. The last stage of mass reduction, which was at 500°C by 25%, could be assumed as a result of further PVA chain degradation [23,24]. There was no further decrease in mass, indicating that only ZnO, Ag, and GO were present. The temperature of calcination process in this study was 500°C for 2 h.

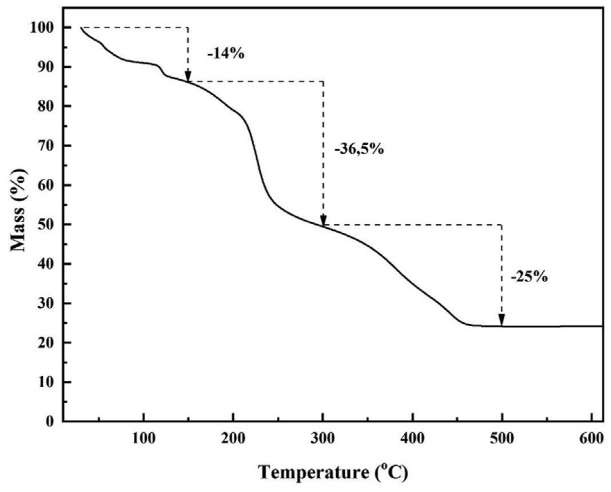

Fig. 5 – TGA thermogam of the PVA/ZnO–Ag-GO nanofiber.

The FT-IR spectra of electrospun and calcined fibres are shown in Fig. 6. All electrospun fibers (ZnO, ZnO–Ag, ZnO-GO, ZnO–Ag-GO had absorption peak characteristics around 3324, 2907, 1707, 1401, 1334, 1088, 916, 842, and 670 cm^{-1} each indicating the presence of O–H (stretching vibration), C–H, C=O, C=C, C=H (stretching vibration), O–H (bending vibration), C–O–C, C=C and Zn–O (bending vibration) respectively [25]. The presence of O–H, C–H(CH_2), and C–O functional groups may occur due to crosslinking between PVA and GO, which can be observed by the presence of absorption peaks at 1100-1000 cm^{-1}; subsequently, this wavenumber also indicated the presence of C–O–C bonding [26]. After the calcination process, most of the absorption peaks showed that PVA characteristics had disappeared and turned into C=C, C–O–C, and Zn–O bonds [27]. In the calcination process the Zn^{2+} and Ag^{+} ions were reduced and ZnO and Ag were formed (Fig. S3). Meanwhile, most of the O–H groups were oxidized to C=C and C=O.

To confirm the XRD diffractogram of the samples, data from the Joint Committee on Powder Diffraction Standards (JCPDS) No. 36–1451 for the hexagonal wurtzite crystal structure for the ZnO, and JCPDS No. 04–0783 for the FCC crystal structure of Ag were used. The XRD patterns of the synthesized nanocomposites are shown in Fig. 7. The results show that ZnO had 2θ of diffraction peaks at 31.8°, 34.4°, 36.2°, 47.5°, 56.5°, 62.9°, 66.4°, 67.9°, 69.1°, 72.6° and 76.9° which have planes of (100), (002), (101), (102), (110), (103), (200), (112), (201), and (004) respectively. This could indicate that the crystal structure of ZnO was hexagonal wurtzite according to JCPDS No.36-1451 [28]. The diffraction pattern of ZnO–Ag-GO nanocomposite showed the presence of 2θ peaks at 38.1°, 44.3°, and 64.4° with (111), (200), and (220) planes respectively and indicated the diffraction pattern of Ag crystal which is an FCC structure according to JCPDS No. 04–0783 [29]. Hence, the results indicate that Ag (symbolised as #) was deposited on the surfaces of both ZnO (symbolised as *) and GO.

Meanwhile, the presence of Ag crystals in ZnO–Ag nanocomposites could not be observed due to the small amount of Ag in the composite and/or the diffraction peak was lower compared to the composition of ZnO. A similar result was also reported by Ravichandran et al., as an example, that the absence of Ag diffraction may be caused by the Ag crystals

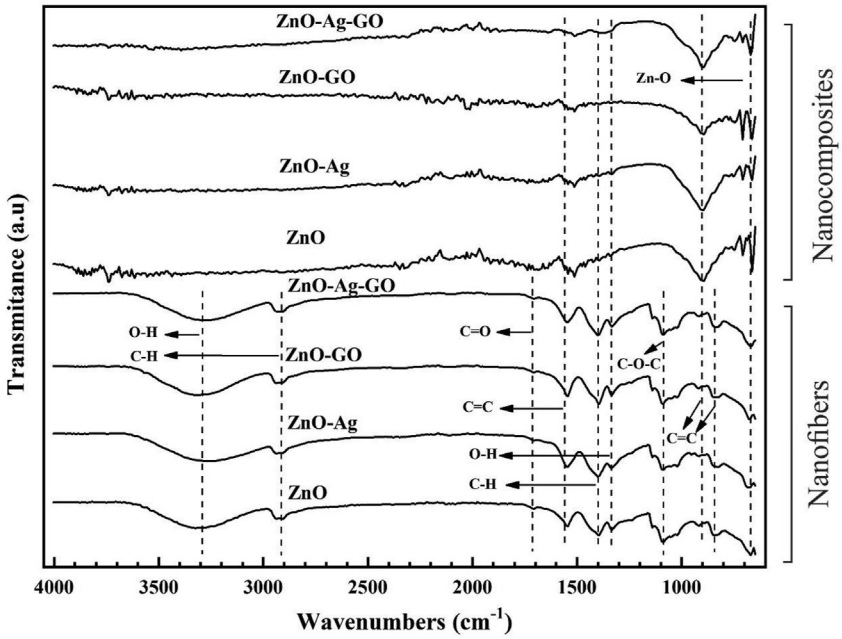

Fig. 6 – Comparison of FT-IR spectra between the electrospun nanofibers and calcined fibers (nanocomposites).

entering the ZnO crystal lattice [30]. Another study has suggested that the reason was due to the strain effect of Ag and Zn crystal lattices as the introduction of silver may lead to distortion of the crystalline structure [31]. Moreover, GO peaks were also not detected in the diffraction pattern of nanocomposites, indicating the insertion of ZnO and Ag nanoparticles. It has been reported that the ZnO and Ag nanoparticles diffuse between adjacent graphene sheets and disturb the distances of the GO layers [30,32]. Another possibility is that the amount of GO in the composites is relatively small. Overall, the diffraction patterns of the nanocomposites showed a co-existence of ZnO, Ag, and GO [33,34]. However, this co-existence has no effects on the ZnO hexagonal wurtzite crystal as it is shown in Figs. 8 and 9.

Based on Fig. 8, the SEM-EDX micrographs of calcined fibres at 500° illustrate that calcination at atmospheric conditions to produce nanocomposite where the surfaces of ZnO and ZnO–Ag-GO were uneven. Based on the EDS spectrum, shown in Fig. 8c, the ZnO–Ag-GO nanocomposite was only composed of ZN, O, Ag, and C. The peak of aluminium appearing in the EDS spectrum, may be originated from the collector wrapped in aluminium foil during the electrospinning process. Nevertheless, this indicated that the synthesis of nanocomposite was performed successfully as it can be observed via the TEM micrographs (Insert in Fig. 9a) and the EDS spectra in Fig. 8c. The TEM micrograph of ZnO–Ag-GO (Fig. 10) showed that the ZnO had a hexagonal wurtzite crystal structure, while Ag had a cubic crystal structure (both of them were also confirmed in the XRD plane system in Fig. 7). Our findings were in accordance with the results reported in previous studies [28,29]. Furthermore, the ZnO crystals had a diameter of 20–30 nm. It could be observed also that Ag nanoparticles were deposited on the surface of ZnO (Fig. 9a), and it appears that GO layers covered the ZnO and Ag nanoparticles (Fig. 9b). Moreover, the GO TEM micrograph showed broad in size with noticeable edges (Fig. 9c).

It has been shown that the photocatalyst characteristics are controlled to great extent by the reduction in electron recombination and the band gap [31]. ZnO, which has an oxygen phase, employs a high probability to perform electron recombination, thus; it is expected to have high electron recombination as well as in GO due the hydroxyl groups. Nevertheless, as it is displayed in Fig. 9, absorption characteristics in interval of 200–430 nm imply the presence of a transition of electrons from valence to conduction bands (O_{2p} → Zn_{3d}). Then, the addition of silver nanoparticles in ZnO–Ag improved the absorption characteristics in the wider visible areas, from 430 to 480 nm [35].

Since the nanocomposites synthesis was carried out by using Ag, it is well known that silver has different refractive index, implying higher reflectance particularly above 400 nm due to surface plasmon resonance (SPR). However, based on Fig. 10, the reflectance decreased in ZnO–Ag as well as in ZnO–Ag-GO compared to those in ZnO or ZnO-GO. It can be therefore assumed that the SPR effect from Ag nanoparticles can increase the absorption characteristics in the visible region [35]. The UV–Vis absorbance spectra of all nanocomposites showed that 90% of the nanocomposites had a reflectance in the visible region. Thus, the determination of absorption properties which correlate to band gap energy (Eg) was carried out on the calcined samples by using the Kubelka–Munk equations [31], and the results are plotted in Fig. S4.

The Eg value of pure ZnO based on a previous study is ~3.37 eV [31]. Table 1 show that the Eg value decreased to 2.75 for ZnO–Ag-GO nanocomposites. This decrease in Eg could be caused by the influence of GO and Ag doping on ZnO lattices, therefore; the gap among the lattices of ZnO is lower, indicating a high electronic level [32]. In this study, however, the Eg value of ZnO–Ag-GO value is slightly smaller than ZnO–Ag with higher wavelength, which indicates a smaller

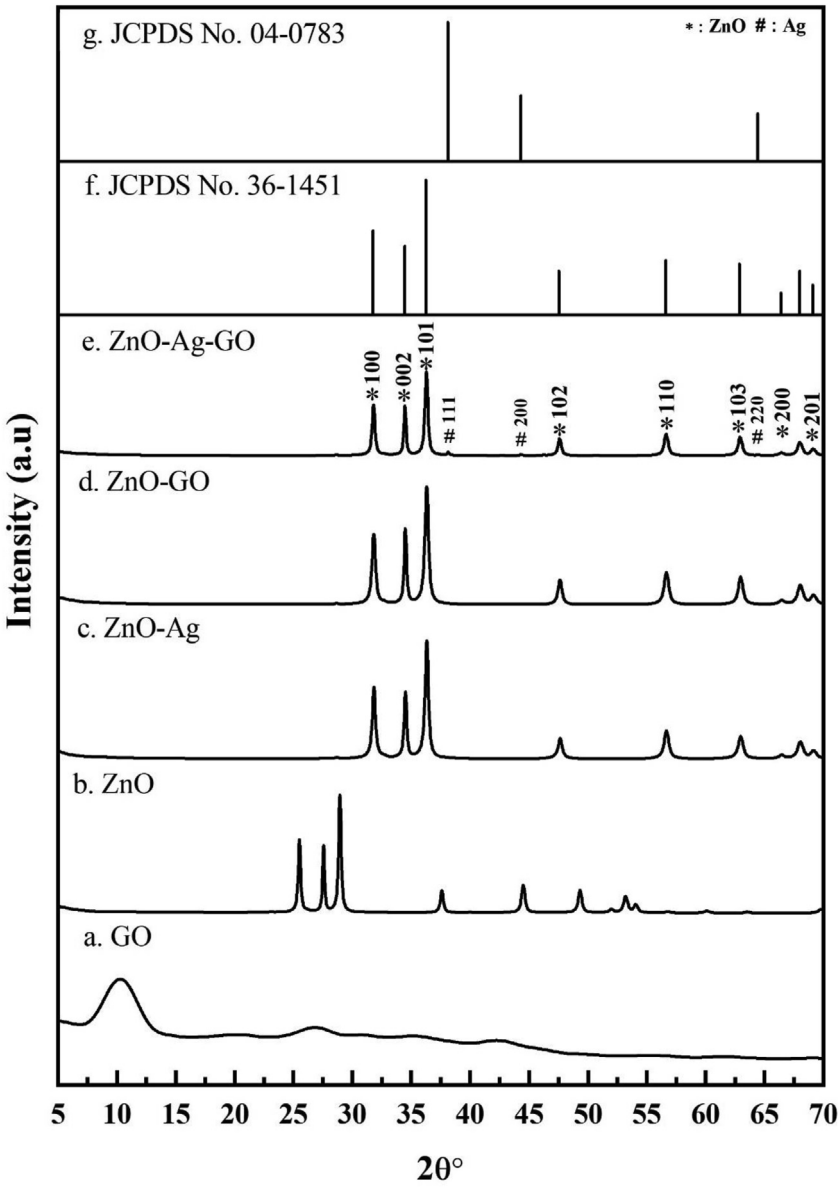

Fig. 7 – XRD patterns of calcined nanocomposites and their comparison to JCPDS standards [28,29].

amount of energy to be used in the activation of photocatalytic species within the ZnO–Ag or ZnO–Ag-GO. In the absence of Ag, the highest Eg value among the samples were calculated with the lowest adsorption wavelength, in contrast; significant wider wavelength was obtained by using silver nanoparticles. Based on the calculation results, the wavelength emitted by the nanocomposite ranged from 417 to 452 nm, indicating the energy activation can be performed in visible light region.

On the other hand, the photocatalytic properties strongly relate to the fluorescent characteristic. The addition of Ag nanoparticles and GO to ZnO nanocomposites resulted in a decrease in PL spectra intensity as can be seen in Fig. 11. The order of effectiveness electron–hole separation for all nanocomposites is as follow: ZnO–Ag-GO > ZnO–Ag > ZnO-GO > ZnO. The addition of Ag and GO contributed importantly in the process of preventing the recombination of electron–hole by acting as an electron trapping site. However, another study implies that the GO does not only act as trapping material, but also as a regulator to manage the electron transfer. Based on TEM micrograph and UV–Vis spectra, a beam of light may arrive on the GO sheets first which have triplet state, allowing the electron to be trapped temporarily [7]. Thus, the electron then is transferred to Ag which has lower Fermi energy compared to ZnO. Subsequently, the electrons from covalence band from ZnO would move quicker to silver nanoparticles. Therefore, this phenomenon indicates an efficient interaction among ZnO, Ag, and GO where electron–hole pairs separate.

The fluorescence characteristics in Fig. 11 showed strong fluorescence emission in 451 nm, 550 nm (green emission), 600 nm, and 750 nm (near infrared range). The peak at 451 nm could be ascribed to the emission of ZnO gap energy as it is determined with the results of Eg by using the Kubelka-Munk

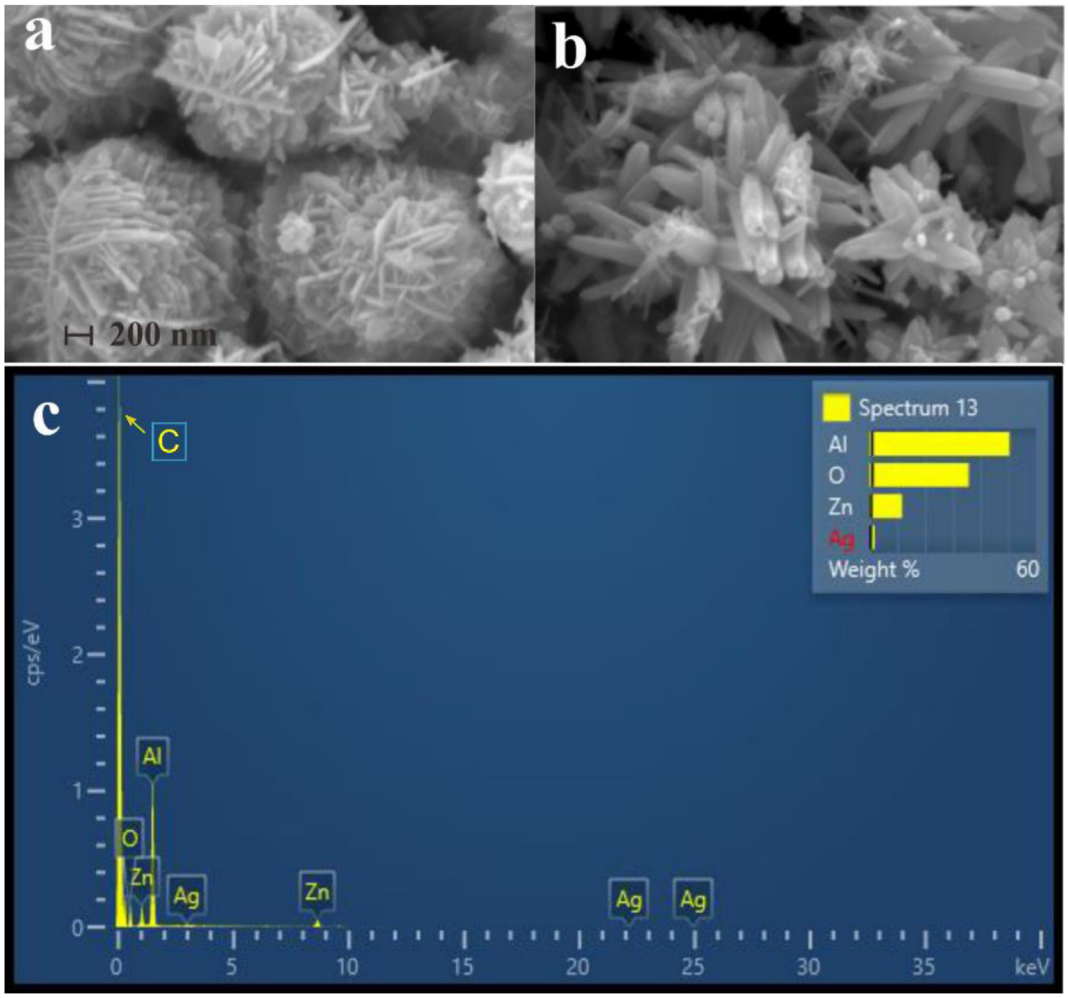

Fig. 8 – SEM-EDX micrographs of (a) ZnO, (b) ZnO–Ag-GO nanocomposites, and (c) EDS spectrum of ZnO–Ag-GO nanocomposite.

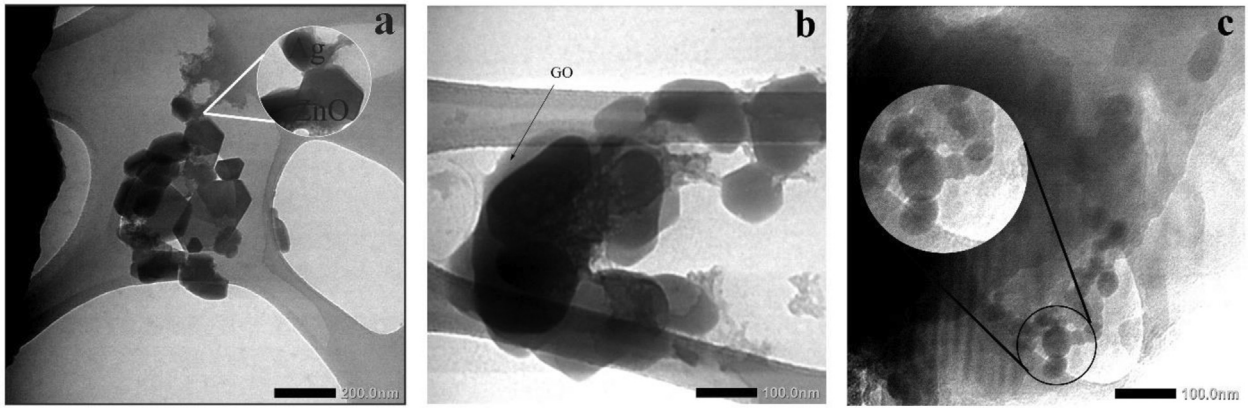

Fig. 9 – TEM micrographs of ZnO–Ag-GO nanocomposites with (a) Hexagonal structure of ZnO attached to Ag in 200 nm, (b) GO layers with Ag in 100 nm, and (c) GO with the absence of ZnO and Ag.

equation [31]. Whilst, the sharp and wide emission peak at 550 nm was due to the chemical defects in ZnO and Oxygen Vacancy (V_o) [29]. The wide emission peak at 600 nm could also be attributed to the oxygen vacancy in ZnO lattices. The defects on the surface of ZnO may act as the centres of electron acceptors or electron traps, the emission peak at 750 nm was considered to be the second order of ZnO gap energy [13].

An illustration of the separation mechanism in ZnO, Ag, and GO nanocomposites is shown in Fig. S5. When the

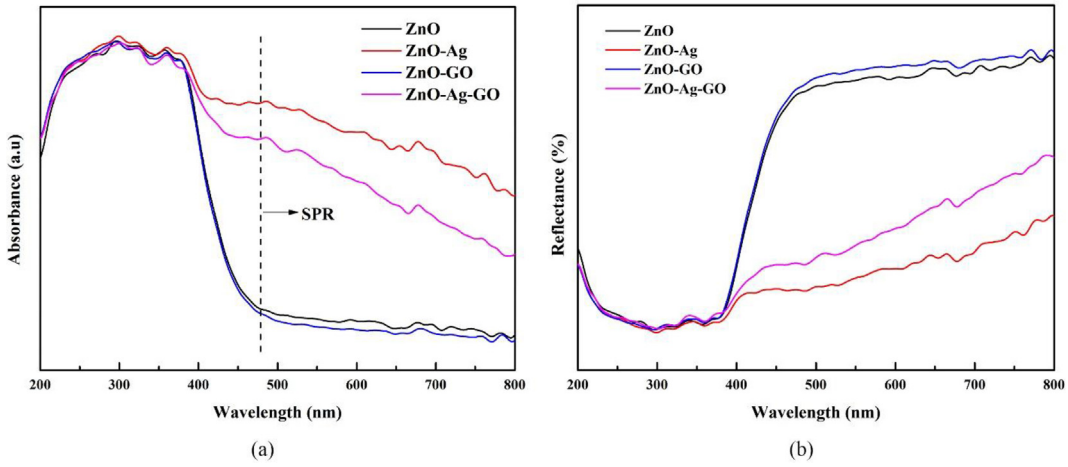

Fig. 10 – UV–Vis spectra of nanocomposites (a) absorbance, and (b) reflectance.

nanocomposite was irradiated by UV/Vis light with a photon energy equal to or greater than the Eg value of ZnO, a charge separation occurred from valence band to conduction band, where the conduction band was e^-, while the valence band was h^+. Electrons in the conduction band of ZnO migrated to Ag and GO sheets where electrons from Ag reacted with O_2 to form $\bullet O_2^-$. Electrons from Ag migrated also to the GO surface and oxidize oxygen to produce $\bullet O_2^-$. The valence band of ZnO holes reacted with H_2O or $-OH^-$ to produce a hydroxyl radical, OH• [20].

Table 1 – Summary of band gaps and BET (Brunaeur-Emmett-Teller) surface areas of the synthesized nanocomposites.

Materials	Band gaps (eV)	λ (nm)	BET surface area (m^2/g)
ZnO	2.98	417	10.134
ZnO–Ag	2.76	450	5.894
ZnO–GO	2.93	424	7.337
ZnO–Ag-GO	2.75	452	8.942

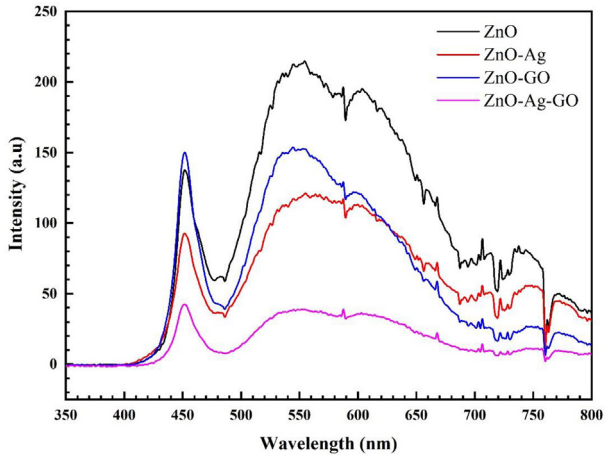

Fig. 11 – Photoluminescence characteristics of ZnO, ZnO–Ag, ZnO-GO, and ZnO–Ag-GO nanocomposites.

Other characteristics that have strong influence in photocatalytic performance are the surface area and pore sizes. This is due to the adsoprtion and desorption mechanisms in the material during isothermic conditions. Fig. 12 shows the N_2 adsorption desorption of the synthesized nanocomposites.

The N_2 adsorption–desorption is a characteristic of mesoporous materials. As the adsorption–desorption measurement carried-out in isothermal conditions, the ratio between before and after being given with pressure or relative pressure (P/P_0) contributes in adsorption–desorption mechanism. According to IUPAC classification, the results of Fig. 12 indicate that all nanocomposites had type IV isotherm with H-1 hysteresis loop. Based on Table 1, the BET surface area showed that the ZnO had 10.134 m^2/g, while the ZnO–Ag-GO had 8.942 m^2/g. This behaviour may be caused due to the addition of GO that has higher porous sizes compared to the Ag nanoparticles. The use of PVA as supporting polymer in $Zn(OAc)_2$ solution reduces Zn^{2+} to Zn^0 as well as Ag^+ to Ag^0 during the electrospinning seems to contribute significantly in the formation of Ag^0. The nanofibers ZnO–Ag-GO that have been calcined in atmospheric condition may oxidize to Zn^0 to form ZnO due its reactivity [36,37]. As the polyols within the PVA have the ability to also reduce the Ag^+, the same reaction may be applied which decomposes the Ag into Ag^0 as well as removing them during high temperature of calcination [23].

On the other hand, the electrospinning process formed nanofibers network with highly porous morphological structure. The beads that are shown in Fig. 3 suggest that the Ag, GO, and Zn were bound together due to PVA. This indicates that both the electrospinning technique and the PVA solution as supporting technique and material respectively, acted as the supporting material. These mechanisms have significant impact to the surface area, which implies to the mesoporous characteristics with diameters of 2–50 nm and had hysteresis loop in the P/P_0 range at 0.3–9.5 with high degree of pore estimator consistency [38]. Thus, a decrease in BET surface area as well as band gap energy implies to the potential characteristics of Zn–Ag-GO as a photocatalytic material with enhanced visible light region.

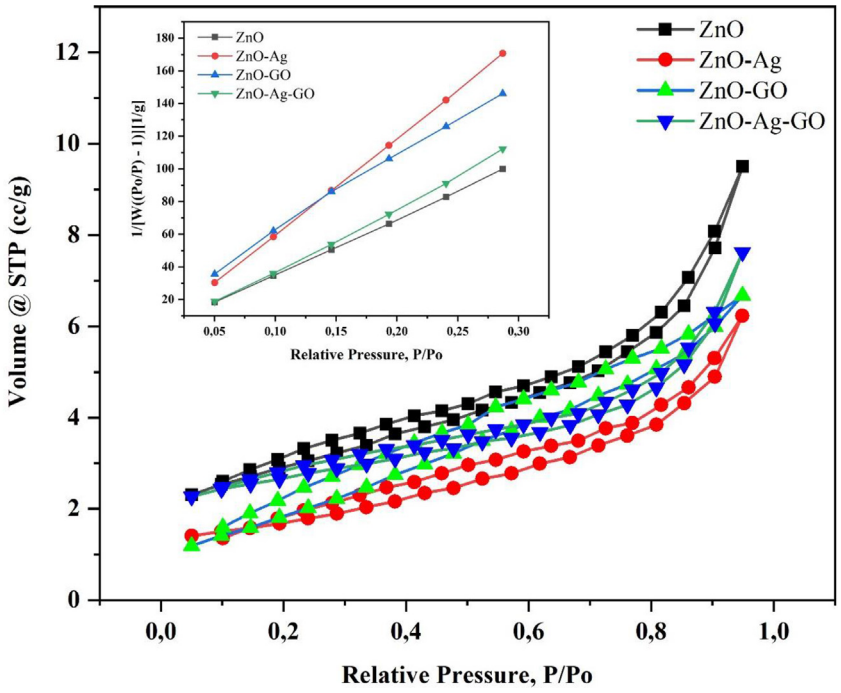

Fig. 12 – N_2 adsorption–desorption isotherm of the synthesized ZnO, ZnO–Ag, ZnO-GO and ZnO–Ag-GO nanocomposites. The internal outline is a BET change-graph of 1/[W(P0/P)-1[1/g] and P/P0.

4. Conclusion

Nanocomposites of ZnO, ZnO–Ag, ZnO-GO and ZnO–Ag-GO have been successfully synthesized by electrospinning followed by calcination process. SEM analysis showed that the spun fibres had a one-dimensional (1D) structure with diameters ranging from 60 to 90 nm. Nanocomposites, produced after calcination process, showed that ZnO, Ag and graphene oxide respectively had hexagonal wurtzite, cubic, and sheet structures. The structures were confirmed by XRD and TEM analysis. Modification of ZnO material with the addition of Ag and GO improved photocatalytic characteristics of ZnO nanocomposites by decreasing electron–hole recombination process, which also could be seen from the reduced value in ZnO band gaps. The results of PL and UV–Vis DRS analysis also showed that the synthesized nanocomposites could be applied in the visible light region. Thus, this study showed an impact of electrospinning technique in enhancing the photocatalytic material particularly in reducing the band gap with certain BET surface areas and wider wavelength region to near visible light.

Funding

Saharman Gea reports article publishing charges was provided by Indonesia Endowment Fund for Education.

Declaration of Competing Interest

All accepted articles will be published only after the signed disclosure statements have been completed. The information will be published as a footnote to the article on the Title page. The authors declare that they have no known competing financial interests or personal relationships that could have appeared to influence the work reported in this paper. The authors declare the following financial interests/personal relationships which may be considered as potential competing interests.

Acknowledgements

The authors would like to thank to the Indonesia Endowment Fund for Education (LPDP) via the scheme of World Class Professor 2021 (No. 2817/E4.1/KK/04.05/2021).

Appendix A. Supplementary data

Supplementary data to this article can be found online at https://doi.org/10.1016/j.jmrt.2022.05.184.

REFERENCES

[1] Duan S, Zhang S, Chang S, Meng S, Fan Y, Zheng X, et al. Efficient photocatalytic hydrogen production from formic acid on inexpensive and stable phosphide/Zn3In2S6 composite photocatalysts under mild conditions. Int J Hydrogen Energy 2019;44(39):21803–20. https://doi.org/10.1016/j.ijhydene.2019.06.179.

[2] Bandekar G, Rajurkar NS, Mulla IS, Mulik UP, Amalnerkar DP, Adhyapak PV. Synthesis, characterization and photocatalytic activity of PVP stabilized ZnO and modified ZnO

nanostructures. Appl Nanosci 2014;4(2):199–208. https://doi.org/10.1007/s13204-012-0189-2.
[3] Mandal SK, Dutta K, Pal S, Mandal S, Naskar A, Pal PK, et al. Engineering of ZnO/rGO nanocomposite photocatalyst towards rapid degradation of toxic dyes. Mater Chem Phys 2018;223:456–65. https://doi.org/10.1016/j.matchemphys.2018.11.002.
[4] Sharma S, Dutta V, Singh P, Raizada P, Rahmani-Sani A, Hosseini-Bandegharaei A, et al. Carbon quantum dot supported semiconductor photocatalysts for efficient degradation of organic pollutants in water: a review. J Clean Prod 2019;228:755–69. https://doi.org/10.1016/j.jclepro.2019.04.292.
[5] Priya B, Shandilya P, Raizada P, Thakur P, Singh N, Singh P. Photocatalytic mineralization and degradation kinetics of ampicillin and oxytetracycline antibiotics using graphene sand composite and chitosan supported BiOCl. J Mol Catal Chem 2016;423:400–13. https://doi.org/10.1016/j.molcata.2016.07.043.
[6] Belver C, Bedia J, Go A, Pen M. Semiconductor photocatalysis for water purification. In: Thomas S, Pasquini D, Leu S-Y, Gopakumar DA, editors. Nanoscale materials in water purification. Madrid, Spain: Elsevier; 2019. p. 581–651. https://doi.org/10.1016/B978-0-12-813926-4.00028-8.
[7] Xue B, Zou Y. High photocatalytic activity of ZnO–graphene composite. J Colloid Interface Sci 2018;529:306–13. https://doi.org/10.1016/j.jcis.2018.04.040.
[8] Nasser R, Othmen WBH, Elhouichet H, Férid M. Preparation, characterization of Sb-doped ZnO nanocrystals and their excellent solar light driven photocatalytic activity. Appl Surf Sci 2017;393:486–95. https://doi.org/10.1016/j.apsusc.2016.09.158.
[9] Mia MNH, Pervez MF, Hossain MK, Reefaz Rahman M, Uddin MJ, Al Mashud MA, et al. Influence of Mg content on tailoring optical bandgap of Mg-doped ZnO thin film prepared by sol-gel method. Results Phys 2017;7:2683–91. https://doi.org/10.1016/j.rinp.2017.07.047.
[10] Hellen N, Park H, Kim KN. Characterization of ZnO/TiO2 nanocomposites prepared via the sol-gel method. J Korean Ceram Soc 2018;55(2):140–4. https://doi.org/10.4191/kcers.2018.55.2.10.
[11] Koutavarapu R, Babu B, Reddy CV, Reddy IN, Reddy KR, Rao MC, et al. ZnO nanosheets-decorated Bi2WO6 nanolayers as efficient photocatalysts for the removal of toxic environmental pollutants and photoelectrochemical solar water oxidation. J Environ Manag 2020;265:110504. https://doi.org/10.1016/j.jenvman.2020.110504.
[12] Yang Y, Li H, Hou F, Hu J, Zhang X, Wang Y. Facile synthesis of ZnO/Ag nanocomposites with enhanced photocatalytic properties under visible light. Mater Lett 2016;180:97–100. https://doi.org/10.1016/j.matlet.2016.05.117.
[13] Ramos PG, Flores E, Luyo C, Sánchez LA, Rodriguez J. Fabrication of ZnO-RGO nanorods by electrospinning assisted hydrothermal method with enhanced photocatalytic activity. Mater Today Commun 2019;19:407–12. https://doi.org/10.1016/j.mtcomm.2019.03.010.
[14] Liu L, Liu Z, Yang Y, Geng M, Zou Y, Shahzad MB, et al. Photocatalytic properties of Fe-doped ZnO electrospun nanofibers. Ceram Int 2018;44(16):19998–20005. https://doi.org/10.1016/j.ceramint.2018.07.268.
[15] Suphankij S, Mekprasart W, Pecharapa W. Photocatalytic of N-doped TiO2 nanofibers prepared by electrospinning. Energy Proc 2013;34:751–6. https://doi.org/10.1016/j.egypro.2013.06.810.
[16] Bose S, Sanyal D. Synthesis and characterization of ZnO microfiber by electrospinning technique. Mater Today Proc 2018;5(3):9860–5. https://doi.org/10.1016/j.matpr.2017.10.178.
[17] Lu F, Wang J, Chang Z, Zeng J. Uniform deposition of Ag nanoparticles on ZnO nanorod arrays grown on polyimide/Ag nanofibers by electrospinning, hydrothermal, and photoreduction processes. Mater Des 2019;181:1–9. https://doi.org/10.1016/j.matdes.2019.108069.
[18] Pascariu P, Airinei A, Olaru N, Olaru L, Nica V. Photocatalytic degradation of Rhodamine B dye using ZnO-SnO2 electrospun ceramic nanofibers. Ceram Int 2016;42(6):6775–81. https://doi.org/10.1016/j.ceramint.2016.01.054.
[19] Gea S, Sari JN, Bulan R, Piliang A, Amaturrahim SA, Hutapea YA. Chitosan/graphene oxide biocomposite film from pencil rod. J Phys Conf 2018;970(1). https://doi.org/10.1088/1742-6596/970/1/012006.
[20] Xu F, Yuan Y, Wu D, Zhao M, Gao Z, Jiang K. Synthesis of ZnO/Ag/graphene composite and its enhanced photocatalytic efficiency. Mater Res Bull 2013;48(6):2066–70. https://doi.org/10.1016/j.materresbull.2013.02.034.
[21] Wang Y, et al. Graphene oxide-IPDI-Ag/ZnO@hydroxypropyl cellulose nanocomposite films for biological wound-dressing applications. ACS Omega 2019;4(13):15373–81. https://doi.org/10.1021/acsomega.9b01291.
[22] Amaturrahim SA, Gea S, Nasution DY, Hutapea YA. Preparation of graphene oxide/bacterial cellulose nanocomposite via in situ process in agitated culture. Asian J Chem 2018;30(7):1564–8. https://doi.org/10.14233/ajchem.2018.21244.
[23] Fievet F, et al. The polyol process: a unique method for easy access to metal nanoparticles with tailored sizes, shapes and compositions. Chem Soc Rev 2018;47(14):5187–233. https://doi.org/10.1039/c7cs00777a.
[24] Gea S, Attaurrazaq B, Situmorang SA, Piliang AFR, Hendrana S, Goutianos S. Carbon-nano fibers yield improvement with iodinated electrospun PVA/silver nanoparticle as precursor via one-step synthesis at low temperature. Polym 2022;14(3). https://doi.org/10.3390/POLYM14030446/S1.
[25] Salehi T, Taherizadeh A, Bahrami A, Allafchian A, Ghafarinia V. Toward a highly functional hybrid ZnO nanofiber–rGO gas sensor. Adv Eng Mater 2020;22(8). https://doi.org/10.1002/adem.202000005.
[26] Işik C, Arabaci G, Ispirli Y, Deveci İ, Teke M. Synthesis and characterization of electrospun PVA/Zn2+ metal composite nanofibers for lipase immobilization with effective thermal , pH stabilities and reusability. Mater Sci Eng C 2019;99:1226–35. https://doi.org/10.1016/j.msec.2019.02.031.
[27] Ghafari E, Feng Y, Liu Y, Ferguson I, Lu N. Investigating process-structure relations of ZnO nanofiber via electrospinning method. Compos B Eng 2017. https://doi.org/10.1016/j.compositesb.2017.02.026.
[28] Neena D, et al. Fabrication of ZnO/N-rGO composite as highly efficient visible-light photocatalyst for 2,4-DCP degradation and H2 evolution. Appl Surf Sci 2019;488:611–9. https://doi.org/10.1016/j.apsusc.2019.05.302.
[29] Koppala S, Xia Y, Zhang L, Peng J, Chen Z, Xu L. Hierarchical ZnO/Ag nanocomposites for plasmon-enhanced visible-light photocatalytic performance. Ceram Int 2019;45(12):15116–21. https://doi.org/10.1016/j.ceramint.2019.04.252.
[30] Ravichandran K, Uma R, Sriram S, Balamurgan D. Fabrication of ZnO:Ag/GO composite thin films for enhanced photocatalytic activity. Ceram Int 2017;43(13):10041–51. https://doi.org/10.1016/J.CERAMINT.2017.05.020.
[31] Pascariu P, et al. Photocatalytic and antimicrobial activity of electrospun ZnO:Ag nanostructures. J Alloys Compd 2020;834:155144. https://doi.org/10.1016/j.jallcom.2020.155144.
[32] Ravichandran K, Uma R, Sriram S, Balamurgan D. Fabrication of ZnO:Ag/GO composite thin films for enhanced

photocatalytic activity. Ceram Int 2017. https://doi.org/10.1016/j.ceramint.2017.05.020.

[33] El-Shafai N, El-Khouly ME, El-Kemary M, Ramadan M, Eldesoukey I, Masoud M. Graphene oxide decorated with zinc oxide nanoflower, silver and titanium dioxide nanoparticles: fabrication, characterization, DNA interaction, and antibacterial activity. RSC Adv 2019;9(7):3704–14. https://doi.org/10.1039/c8ra09788g.

[34] Ata S, et al. Graphene and silver decorated ZnO composite synthesis, characterization and photocatalytic activity evaluation. Diam Relat Mater 2018;90:26–31. https://doi.org/10.1016/j.diamond.2018.09.015.

[35] Kanimozhi G, Vinoth S, Kumar H, Srinadhu ES, Satyanarayana N. Electrospun nanocomposite Ag–ZnO nanofibrous photoanode for better performance of dye-sensitized solar cells. J Electron Mater 2019;48(7):4389–99. https://doi.org/10.1007/s11664-019-07199-2.

[36] Philip MR, Nguyen HPT, Babu R, Krishnakumar V, Bui THQ. Polyol synthesis of zinc oxide-graphene composites: enhanced dye- sensitized solar cell efficiency. Curr Nanomat May 2018;3(1):52–60. https://doi.org/10.2174/2405461503666180507124310.

[37] Rao BG, Mukherjee D, Reddy BM. Novel approaches for preparation of nanoparticles. In: Nanostructures for novel therapy: synthesis, characterization and applications; 2017. p. 1–36. https://doi.org/10.1016/B978-0-323-46142-9.00001-3.

[38] Wang S, Kuang P, Cheng B, Yu J, Jiang C. ZnO hierarchical microsphere for enhanced photocatalytic activity, 741. Elsevier B.V.; 2018. https://doi.org/10.1016/j.jallcom.2018.01.141.